UDC 621.314 https://doi.org/10.20998/2074-272X.2025.2.04

Z. Darsouni, S.E. Rezgui, H. Benalla, F. Rebahi, M.A.M. Boumandjel

Ensuring service continuity in electric vehicles with vector control and linear quadratic regulator for dual star induction motors

Introduction. *In this paper, the use of a Linear Quadratic Regulator (LQR) to control a Dual Star Induction Motor (DSIM) powered by dual three-level neutral point clamped inverters in electric vehicle (EV) propulsion systems is explored.* ***Purpose.*** *Ensuring both high performance against parameter sensitivity and service continuity in the event of faults is challenging in EV propulsion systems. The* ***aim*** *is to maximize both system performance and service continuity through the optimal design of the controller.* ***Methods.*** *DSIM is controlled by a LQR, which is replaced the traditional PI controller in the field-oriented control (FOC) system for speed regulation. Starting with FOC the optimal regulator is designed by introducing a minimization criterion into the Ricatti equation. The LQR control law is then employed as a speed regulator to ensure precise regulation and optimize DSIM operation under various load and speed conditions. The avoidance of linearization of the DSIM facilitates the exploitation of its true nonlinear dynamics.* ***Novelty.*** *Three tests are conducted to evaluate system performance. A precision test by varying the reference speed and analyzing speed response, settling time, precision and overshoot, a robustness test against parameter variations, assessing system robustness against changes in stator and rotor resistances and moment of inertia, and a fault robustness test evaluating system robustness against faults such as phase faults while maintaining load torque. The* ***results*** *show that this approach can keep the motor running smoothly even under parameter variations or degraded conditions. The precision and adaptability of the LQR technique enhance the overall efficiency and stability of the DSIM, making it a highly viable solution for modern EVs. This robust performance against parameter variations and loads is essential in ensuring the reliability and longevity of EV propulsion systems.* ***Practical value****. This approach holds significant potential for advancing EV technology, promising improved performance and reliability in real-world applications.* References 44, tables 2, figures 15.

Key words: **dual star induction motor, linear quadratic regulator, neutral point clamped, electric vehicle, field-oriented control.**

Вступ. *У цій статті досліджується використання лінійного квадратичного регулятора (LQR) для керування асинхронним двигуном із подвійною зіркою (DSIM), що живиться від подвійних трирівневих інверторів із закріпленням нейтральної точки в силових системах електромобілів.* ***Призначення***. *Забезпечення як високої продуктивності щодо чутливості до параметрів, так і безперервності роботи в разі несправностей є складним завданням для силових систем електромобілів.* ***Метою*** *є максимізація як продуктивності системи, так і безперервності обслуговування за допомогою оптимальної конструкції контролера.* ***Методи***. *DSIM керується LQR, який замінює традиційний PI-контролер у системі орієнтованого на поле керування (FOC) для регулювання швидкості. Починаючи з FOC, оптимальний регулятор розробляється шляхом введення критерію мінімізації в рівняння Рікатті. Потім закон керування LQR використовується як регулятор швидкості для забезпечення точного регулювання та оптимізації роботи DSIM за різних умов навантаження та швидкості. Уникнення лінеаризації DSIM полегшує використання його справжньої нелінійної динаміки.* ***Новизна***. *Для оцінки продуктивності системи проводяться три тести. Випробування на точність шляхом зміни еталонної швидкості та аналізу відповіді на швидкість, часу встановлення, точності та перерегулювання, випробування на стійкість щодо варіацій параметрів, оцінювання стійкості системи щодо змін опору статора та ротора та моменту інерції, а також тест на стійкість до несправностей, що оцінює стійкість системи проти несправностей, таких як замикання фаз, зберігаючи момент навантаження.* ***Результати*** *показують, що цей підхід може підтримувати безперебійну роботу двигуна навіть за коливань параметрів або погіршених умов. Точність і адаптивність техніки LQR підвищують загальну ефективність і стабільність DSIM, що робить його дуже життєздатним рішенням для сучасних електромобілів. Ця надійна робота проти коливань параметрів і навантажень є важливою для забезпечення надійності та довговічності силових систем електромобілів.* ***Практична цінність***. *Цей підхід має значний потенціал для вдосконалення технології електромобілів з точки зору покращеної продуктивності і надійності у реальних прикладах.* Бібл. 44, табл. 2, рис. 15.

Ключові слова: **асинхронний двигун з подвійною зіркою, лінійно-квадратичний регулятор, зафіксована нейтральна точка, електромобіль, керування з орієнтацією за полем.**

Introduction. Preserving the environment is a top priority in today's world. Pollution and climate change are forcing us to reconsider the way we travel. Electric Vehicles (EVs) unquestionably represent an efficient measure and a promising solution to this problem [1]. In the world of EVs, the core of this technology lies in their propulsion system, which separates it from combustion vehicle. It contains [2] (Fig. 1):

- the battery, which is an energy storage unit that powers the electric motor for vehicle propulsion. Often, EVs are equipped with Battery Management System (BMS) that supervise the performance of the battery and motor, optimize energy efficiency, and ensure safe operation;
- the electric motor is responsible for converting electric energy into mechanical energy to drive the vehicle's wheels;
- the inverter is an electronic converter that controls the direction and power of the electric current supplied to the motor;
- the embedded control system, that control the inverter state and hence the direction and the speed of the vehicle.

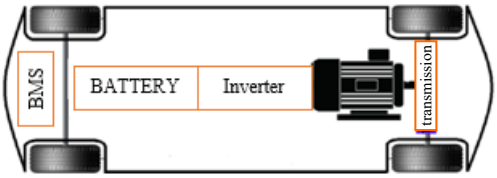

Fig. 1. Powertrain of EV

To control any AC motor, an essential step called Field-Oriented Control (FOC) is used. FOC allows us to decouple the electromagnetic torque from the flux, making AC motors behave similarly to DC motors [3]. This technique provides several advantages, including high efficiency, better torque control at low speeds, smooth operation, a wide speed range, and improved dynamic response [4]. Nevertheless, FOC requires an estimator to calculate angular velocity feedback for speed control [5].

Purpose. This paper aims to maximize the performance of EVs by improving the powertrain of the EV, and to do so a comparison between regulators such as

Sliding Mode Control (SMC) regulator, Model Reference Adaptive Control (MRAC) regulator and Linear Quadratic Regulator (LQR) to choose the most appropriate one. In the context of ensuring service continuity of EVs, it is essential to choose an appropriate type of motors from the commonly used types that are AC and DC motors.

Brushless (BLDC) motor. With the elimination of brushes, the BLDC motor has emerged as a solution to the old DC motor. This type of motor offers improved efficiency and requires less maintenance [6, 7]. Additionally, it has the ability to provide higher torque and power over a wide operating range, compared to the older DC motor. However, the BLDC motor has a relatively limited field weakening capability. Furthermore, high speeds pose a safety risk due to the potential for magnet breakage. They are also sensitive to high temperatures, which affects the overall motor performance [6, 8]. While the BLDC motor offers various advantages as mentioned, it may not ensure service continuity in the presence of motor faults, which make it not the most suitable motor in this case.

Induction motor. The simple structure, high reliability, robustness, reduced maintenance, low cost, and operation even in adverse conditions are all advantages that led Tesla Company to choose this type of motors for the Tesla S model [6]. Additionally, these motors offer an extended speed range through flux weakening in the constant power zone, as well as absence of commutation and the ability to recover energy during the braking phase [9, 10].

However, controlling this type of motor is also challenging, as it requires precise balancing of slip percentages and load quantity to ensure efficient operation at all times [6]. Additionally, while losses increase at high speeds, its efficiency decreases at both low and high speeds [8]. Furthermore, if the critical synchronous speed is reached, the motor may fail [11, 12]. In the context of selecting more suitable motor for an electric car to ensure continuous service, it appears that induction motors are not the optimal choice for this scenario.

Dual Star Induction Motor (DSIM). The robustness and low maintenance of the DSIM allow for the gradual replacement of the induction motor in industrial applications, even in high power scenarios such as railway traction, marine propulsion [13–15]. This type of motor consists of two windings with phases shifted by 30 electric degrees from each other, powered by a 6-phase inverter or 2 inverters of 3 phases [16].

Among its advantages, one can also note a higher torque density compared to traditional induction motors. Additionally, the DSIM reduces harmonic content and exhibits high reliability, allowing it to operate even in the presence of faults on one or more phases of the motor [17, 18]. It also offers power segmentation, minimizing torque ripple and rotor losses while reducing harmonic currents [19]. However, controlling the DSIM is considered complex, especially regarding achieving torque and flux decoupling [16, 17]. Despite this drawback, this type of motor is capable of operating under degraded conditions [20, 21]. In comparison between BLDC, induction motor and DSIM the last one stands out as the most suitable option for EVs in most scenarios and, particularly in ensuring service continuity.

Control methods. There are numerous control techniques classified into 2 categories: classic techniques and advanced techniques.

Starting with classical ones, the indirect and direct (IFOC and FOC) was proposed for the first time by K. Hasse in 1968 and Werner Leonard in 1971 [22], as a replacement for classic correctors. Many researches have focused on these 2 techniques [23–27], applying them to different types of machines, and according to the results obtained: FOC and IFOC control allow for control over the machine's flux and torque. They have a better effect on suppressing high-order harmonics, reference tracking with a good response time, and high precision in steady state. However, they are sensitive to parametric variations, and the transformation of variables is based on an estimator, making it sensitive [28]. For the several mentioned disadvantages, many researchers were proposed such as SMC, MRAC and optimal control with LQR to enhance FOC and mitigate high sensitivity to parameters variations, and ensure fault tolerant control [29].

SMC is intended for systems with variable structures because it is robust to parameter changes or parameter uncertainty and total suppression of external disturbances [30–32]. It provides also good reference tracking with fast response time [33]. On one hand, high-frequency switching causes chattering phenomenon which significantly affects the overall system performance. Additionally, it suffers from overshoot peaks and high stabilization times. Finally, it does not guarantee good performance in the presence of disturbances such as sudden changes in reference speed [30, 34].

MRAC is used to control systems with variable structures or unknown parameters [35, 36]. Many research has been conducted on MRAC and applied to various types of motors [37–40]. According to simulation results, MRAC is robust against parameter uncertainties such as stator and rotor resistance (R_s, R_r) and moment of inertia (J) [41], as well as parameter changes [42], and presents a good reference tracking and precision [37, 38, 40]. However, it suffers from high overshoot [42, 43], complexity and heavy computational time of the algorithms [41]. Real-time parameter updates lead to oscillations in the response and influence the desired dynamic response [43].

Optimal control. Thanks to its robustness, the LQR control has been widely used in the industry, especially from the 2000s to the present day [44]. It is based on maximizing or minimizing a performance criterion (depending on how the Hamiltonian is defined) [37]. Studies have already been conducted on the LQR control [38, 39, 44], where simulation results have shown that this technique offers high performance by eliminating the gap in the state trajectory. It also allows for tracking the reference with zero steady-state error in a settling time of less than one second, and with minimal effort [39]. Carried out robustness testing against parameter uncertainties and external disturbances, where the LQR control showed very satisfactory performance, with tolerance ranging from 30 % to 90 % uncertainty and complete rejection of external disturbances.

However, the only inevitable issue when designing an LQR controller for different dynamics lays in the systematic determination of the parameters of the performance matrices Q and R [44]. Therefore, it can be said that optimal control is a promising choice to control an EV.

This contribution not only focuses on ensuring high performance of the EV, but also on service continuity by combining the advantages of the DSIM and LQR. By leveraging the strengths of both LQR and the DSIM, such as precise speed tracking, minimal overshoot and high precision offered by LQR, along with the capability of working with DSIM even under phase faults, this approach ensures a seamless operation of the EV system, maintaining superior performance and robustness in various operating conditions.

Given the comparison above, the DSIM will be controlled by a LQR, which will replace the traditional PI controller in the FOC system for speed regulation.

Modeling of the DSIM. The stator consists of two pairs of windings shifted by 30°, and a short-circuited rotor as a classical induction motor. The spatial representation of the windings of the DSIM is illustrated on the Fig. 2, where L_r, L_s are the rotor and stator inductances, R_r, R_s are the rotor and stator resistances.

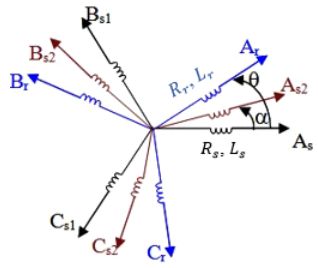

Fig. 2. Spatial representation of the DSIM windings

The dynamic of the DSIM in the *d-q* reference can be divided into three categories of equations.

1) Electric equations:

$$\begin{cases} V_{ds1} = R_{s1} i_{ds1} + \mathrm{d}\Phi_{ds1}/\mathrm{d}t - \omega_s \Phi_{qs1}; \\ V_{ds2} = R_{s2} i_{ds2} + \mathrm{d}\Phi_{ds2}/\mathrm{d}t - \omega_s \Phi_{qs2}; \\ V_{qs1} = R_{s1} i_{qs1} + \mathrm{d}\Phi_{qs1}/\mathrm{d}t + \omega_s \Phi_{ds1}; \\ V_{qs2} = R_{s2} i_{qs2} + \mathrm{d}\Phi_{qs2}/\mathrm{d}t + \omega_s \Phi_{ds2}; \\ 0 = R_r i_{dr} + \mathrm{d}\Phi_{dr}/\mathrm{d}t - (\omega_s - \omega_r)\Phi_{qr}; \\ 0 = R_r i_{qr} + \mathrm{d}\Phi_{qr}/\mathrm{d}t + (\omega_s - \omega_r)\Phi_{dr}, \end{cases} \quad (1)$$

where V_{ds1}, V_{qs1}, V_{ds2}, V_{qs2} are respectively the stator voltages in the *d-q* axis; R_{s1}, R_{s2} are the stator resistances; L_{s1}, L_{s2} are the stator inductances; i_{ds1}, i_{qs1}, i_{ds2}, i_{qs2} are the components of the stator currents in the *d-q* axis; i_{dr}, i_{qr} are the rotor currents in the *d-q* axis; Φ_{ds1}, Φ_{qs1}, Φ_{ds2}, Φ_{qs2} are the components of the stator flux in the *d-q* axis; Φ_{dr}, Φ_{qr} are the rotor fluxes in the *d-q* axis; R_r is the rotor resistance; ω_s, ω_r are the stator and rotor angular speeds.

2) Magnetic equations:

$$\begin{cases} \Phi_{ds1} = L_{s1} i_{ds1} + L_m (i_{ds1} + i_{ds2} + i_{dr}); \\ \Phi_{ds2} = L_{s2} i_{ds2} + L_m (i_{ds1} + i_{ds2} + i_{dr}); \\ \Phi_{qs1} = L_{s1} i_{qs1} + L_m (i_{qs1} + i_{qs2} + i_{qr}); \\ \Phi_{qs2} = L_{s2} i_{qs2} + L_m (i_{qs1} + i_{qs2} + i_{qr}); \\ \Phi_{dr} = L_r i_{dr} + L_m (i_{ds1} + i_{ds2} + i_{dr}); \\ \Phi_{qr} = L_r i_{qr} + L_m (i_{qs1} + i_{qs2} + i_{qr}), \end{cases} \quad (2)$$

where L_r is the rotor inductance; L_m is the mutual inductance.

3) Mechanical equations.

The electromagnetic torque is given as:

$$C_{em} = p\left(\Phi_{ds1} i_{qs1} - \Phi_{qs1} i_{ds1} + \Phi_{ds2} i_{qs2} - \Phi_{qs2} i_{ds2}\right), \quad (3)$$

where p is the number of pole pairs.

The rotation dynamic is given as:

$$\frac{\mathrm{d}\Omega}{\mathrm{d}t} = \frac{1}{J}\left(C_{em} - C_r - F_r \cdot \Omega\right), \quad (4)$$

where Ω is the rotor angular speed; J is the moment of inertia; C_r is the load torque; F_r is the friction coefficient.

Modeling of the three levels neutral point clamped (NPC) inverter. Figure 3 illustrates a three-level inverter. A multi-level inverter typically contains $(n–1)$ capacitors in the DC link, $(n–1)(n–2)$ clamping diodes, and $2(n–1)$ switches. Therefore, a three-level inverter requires 2 balancing capacitors, 2 clamping diodes, and 4 switches multiplied by 3 (number of phases). This gives us a total of 6 diodes and 12 switches. Table 1 summarizes the possible switching sequences.

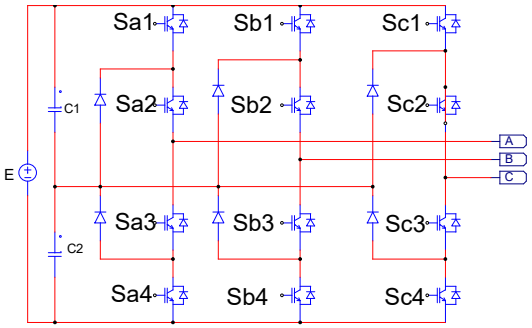

Fig. 3. Three phases three levels NPC inverter

Table 1

Possible sequences of three levels NPC inverter

K_1	K_2	K_3	K_4	V_{a0}
1	1	0	0	$E/2$
0	1	1	0	0
0	0	1	1	$–E/2$

Optimal control by LQR. In this section, instead of using PI regulator, the LQR will be used as a speed regulator to ensure service continuity and robustness against parameters variations. To accomplish this, several steps will be taken, beginning with the general state space representation of the DSIM:

$$\begin{cases} [\dot{x}(t)] = [A]\cdot[x(t)] + [B]\cdot[u(t)]; \\ [y(t)] = [C]\cdot[x(t)] + [D]\cdot[u(t)], \end{cases} \quad (5)$$

where $[x(t)]$ is the state variable matrix, $x \in \Re^n$; $[A]$ is the state parameters matrix, $A \in \Re^{n\times n}$; $[B]$ is the control matrix, $B \in \Re^{n\times m}$; $[u(t)]$ is the control vector, $u \in \Re^m$; $[C]$ is the observation matrix; $[D]$ is the direct action matrix; $[y(t)]$ is the output matrix. While:

$$[x(t)] = \begin{bmatrix} \Phi_{ds1} & \Phi_{ds2} & \Phi_{qs1} & \Phi_{qs2} & \Phi_{dr} & \Phi_{qr} \end{bmatrix}^T;$$

$$[u(t)] = \begin{bmatrix} V_{ds1} & V_{ds2} & V_{qs1} & V_{qs2} & 0 & 0 \end{bmatrix}^T.$$

The optimality criterion can be expressed as:

$$j(u(t)) = \int_0^\infty \left[x^T \cdot Q \cdot x + u^T \cdot R \cdot u\right] \mathrm{d}t. \quad (6)$$

In the case there are constraints, to obtain the optimal feedback coefficient, we must solve the following Ricatti matrix equation:

$$A^T \cdot P + P \cdot A - P \cdot B \cdot R^{-1} \cdot B^T \cdot P + Q = 0. \quad (7)$$

The introduction of the minimization criterion in Ricatti equation make it as follows:

$$A^T \cdot P + P \cdot A - P \cdot B \cdot R^{-1} \cdot B^T \cdot P + C^T \cdot Q \cdot C = 0. \quad (8)$$

While:

$$R = 0.1 \cdot \begin{bmatrix} 1 & 1 & 1 & 1 & 1 & 1 \\ 1 & 1 & 1 & 1 & 1 & 1 \\ 1 & 1 & 1 & 1 & 1 & 1 \\ 1 & 1 & 1 & 1 & 1 & 1 \\ 1 & 1 & 1 & 1 & 1 & 1 \\ 1 & 1 & 1 & 1 & 1 & 1 \end{bmatrix}; \quad Q = 2 \cdot \begin{bmatrix} 1 & 0 & 0 & 0 & 0 & 0 \\ 0 & 1 & 0 & 0 & 0 & 0 \\ 0 & 0 & 1 & 0 & 0 & 0 \\ 0 & 0 & 0 & 1 & 0 & 0 \\ 0 & 0 & 0 & 0 & 1 & 0 \\ 0 & 0 & 0 & 0 & 0 & 1 \end{bmatrix};$$

$$B = \begin{bmatrix} 1 & 0 & 0 & 0 & 0 & 0 \\ 0 & 1 & 0 & 0 & 0 & 0 \\ 0 & 0 & 1 & 0 & 0 & 0 \\ 0 & 0 & 0 & 1 & 0 & 0 \\ 0 & 0 & 0 & 0 & 0 & 0 \\ 0 & 0 & 0 & 0 & 0 & 0 \end{bmatrix};$$

$$C = \begin{bmatrix} \frac{\alpha_1}{\gamma} & \frac{-L_m L_r}{\gamma} & 0 & 0 & \frac{-L_m}{\delta} & 0 \\ \frac{-L_m L_r}{\gamma} & \frac{\alpha_1}{\gamma} & 0 & \frac{-L_m}{\delta} & 0 & 0 \\ 0 & 0 & \frac{\alpha_2}{\gamma} & \frac{-L_m L_r}{\gamma} & 0 & \frac{-L_m}{\delta} \\ 0 & 0 & \frac{-L_m L_r}{\gamma} & \frac{\alpha_2}{\gamma} & 0 & \frac{-L_m}{\delta} \\ \frac{-L_m}{\delta} & \frac{-L_m}{\delta} & 0 & 0 & \frac{2L_m L_s}{\delta} & 0 \\ 0 & 0 & \frac{-L_m}{\delta} & \frac{-L_m}{\delta} & 0 & \frac{2L_m L_s}{\delta} \end{bmatrix},$$

where:

$$\alpha_1 = L_m \cdot L_r + L_m \cdot L_{s1} + L_r \cdot L_{s1};$$
$$\alpha_2 = L_m \cdot L_r + L_m \cdot L_{s2} + L_r \cdot L_{s2};$$
$$\gamma = L_m \cdot L_s^2 + L_r \cdot L_s^2 + 2 \cdot L_m \cdot L_r \cdot L_s;$$
$$\delta = 2 \cdot L_m \cdot L_r + L_m \cdot L_s + L_r \cdot L_s;$$
$$L_s = L_{s1} = L_{s2},$$

where L_m is the magnetizing inductance.

The optimal gain can be expressed as:

$$K_{opt} = -R^{-1} \cdot B^T \cdot P. \quad (9)$$

New optimal gain will be calculated starting from K_{opt} which will equal the sum of elements of K_{opt}

$$K_{1opt} = \sum K_{opt}. \quad (10)$$

The control law equal:

$$U_{opt} = -K_{1opt} \cdot [X]. \quad (11)$$

As K_{1opt} is defined, also U_{1opt} will also be defined in the same way:

$$U_{1opt} = \sum U_{opt}. \quad (12)$$

The optimal controller will be used in the control loop as shown in Fig. 4, the global control scheme – in Fig. 5.

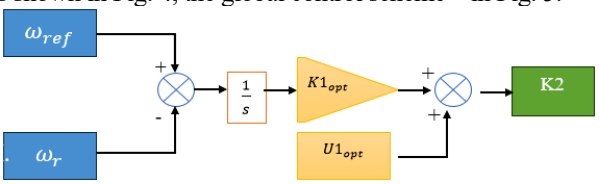

Fig. 4. Optimal control loop

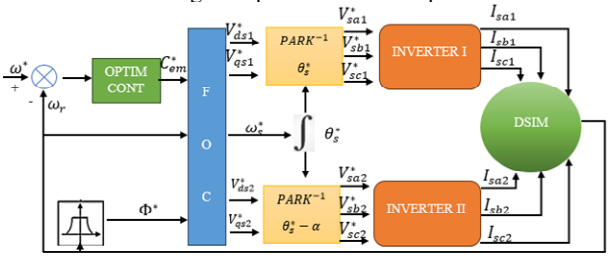

Fig. 5. LQR global regulation loop with FOC

Simulation results. The simulation investigates into the evaluation of the LQR implemented on a control system of the DSIM. It includes 3 distinct tests.

Test 1. The precision in tracking reference speed, settling time, and overshoot are examined to gauge the regulator's performance under different conditions.

Test 2. The regulator's resilience against parameter variations such as stator resistance, rotor resistance and inertia under load torque conditions is tested, aiming to ensure stable operation amidst the fluctuations that are encountered in the real world.

Test 3. The simulation examines the regulator and the DSIM robustness against phase disturbances for enhancing its reliability in practical scenarios.

Through these meticulous assessments, valuable insights are gained into the effectiveness and durability of the LQR regulator in controlling the DSIM system across diverse operating conditions in objective to ensure service continuity and high performance against parameters variations and external disturbances.

The parameters of the DSIM used in this study are defined in Table 2.

Table 2

Parameters of the DSIM

Parameter	Value	Parameter	Value
R_s, Ω	3.72	L_r, H	0.006
R_r, Ω	2.12	L_m, H	0.4092
L_s, H	0.022	J, kg·m^2	0.0625
p	1	F_r	0.001

Test 1. Speed tracking and disturbance rejection. The motor is initiated with a reference speed $\omega_{ref} = 200$ rad/s (Fig. 6). The response shows a settling time of 0.25 s, without overshoot and a precision level of 99 %. At the moment of 0.5 s, the speed reference is transitioned to 300 rad/s. Clearly, the system demonstrates the same stabilizing time of 0.25 s, coupled with an absence of overshoot (0 %) with a precision level of 99 %. These results underscore the LQR regulator's particular ability to quickly and accurately track reference speed changes.

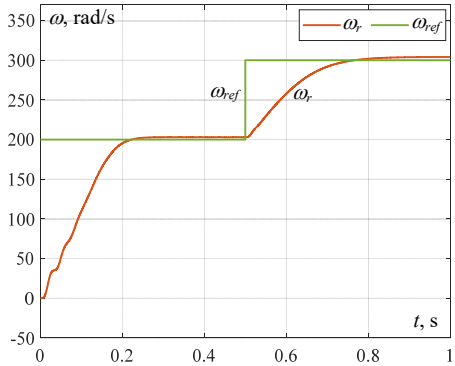

Fig. 6. Performance evaluation of LQR regulator in tracking

The current curves are observed to be non-ideal sinusoidal waveform and shifted by 120° (Fig. 7, 8). The currents of the second stator are shifted by 30° from the first stator. During the first 0.25 s, the currents undergo a transient phase before stabilizing at a peak value of 29 A. Then, at $t = 0.5$ s, the reference speed undergoes a sudden transition, reaching 300 rad/s. This change in speed results in a change in power, according to the relationship $P = C_{em} \cdot \Omega$. Consequently, the currents also evolve, reaching a lower peak value of 20 A in response to the change in speed.

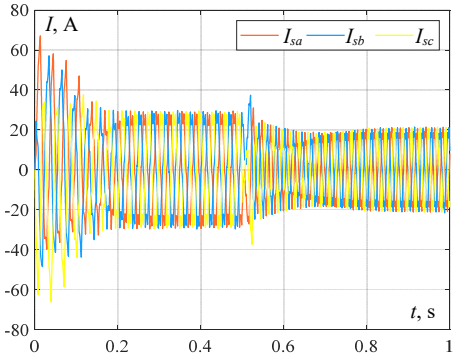

Fig. 7. Stator 1 currents

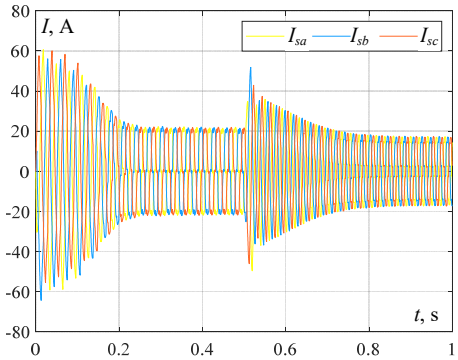

Fig. 8. Stator 2 currents

Figure 9 illustrates the response of the DSIM controlled by an LQR regulator. Initially, the system starts unloaded with a reference speed set to 150 rad/s. The DSIM reaches this target speed rapidly, within 0.2 s, achieving a precision of 99 %, with a resulting speed of 151.5 rad/s. At t = 0.5 s, a resistant torque of 10 N·m is applied, causing the speed to decrease to 148.8 rad/s. When the load torque is removed at t = 1 s, the speed recovers to 151.5 rad/s. Despite these disturbances, the DSIM demonstrates robust performance, maintaining a response precision of 99 %.

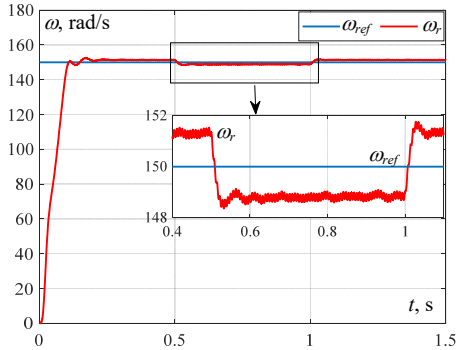

Fig. 9. Speed response of DSIM under load torque

Figure 10 shows that depicts the system's response when load torque is introduced at 0.5 s. DSIM promptly generates an electromagnetic torque equal to load torque. At t = 1 s, when the load torque is removed, the electromagnetic torque returns to 0. The system demonstrates a stabilization time of 0.1 s in both scenarios. Notably, small ripples of approximately ±8 N·m are observed around the generated torque, indicating minor fluctuations. This response highlights the DSIM's ability to swiftly adapt to load torque changes while maintaining overall stability within a tight time frame.

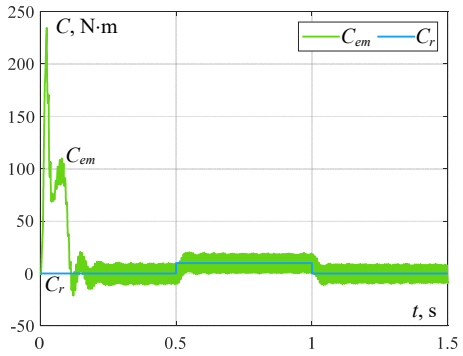

Fig. 10. DSIM torque response to load torque introduction

Test 2. Parameter variations evaluation. The simulation (Fig. 11–13) shows the response of the DSIM controlled with LQR regulator under parameters variations such as J, R_s and R_r. Initially, the motor operates with parameters R_s = 3.72 Ω, R_r = 2.12 Ω and J = 0.0625 kg·m^2. When these parameters are multiplied by 1.5 at instant t = 0.5 s, the new values become R_s = 5.58 Ω, R_r = 3.18 Ω and J = 0.09375 kg·m^2. Then, at t = 1 s, the parameters are doubled, resulting in R_s = 7.44 Ω, R_r = 4.24 Ω and J = 0.125 kg·m^2. Despite these substantial variations, the motor maintains stable performance in all scenarios. This constancy demonstrates the robustness of LQR controller against parametric changes, highlighting its ability to effectively regulate the system and minimize deviations from the set point, regardless of the conditions, thus ensuring precise and stable control of the system in changing conditions.

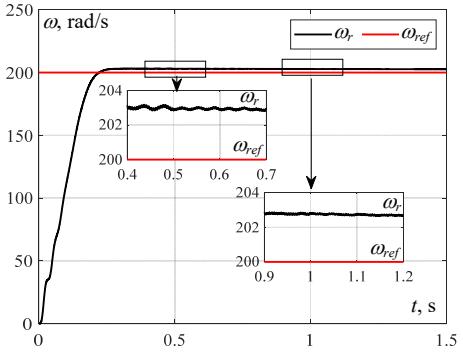

Fig. 11. Motor response under moment of inertia variations

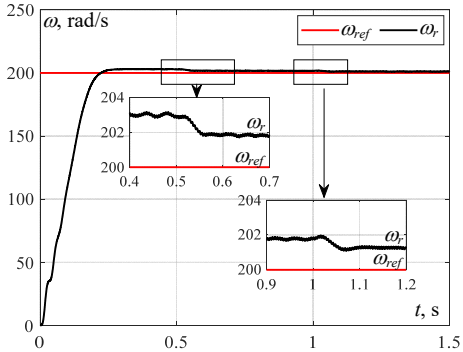

Fig. 12. Motor response under stator resistance variations

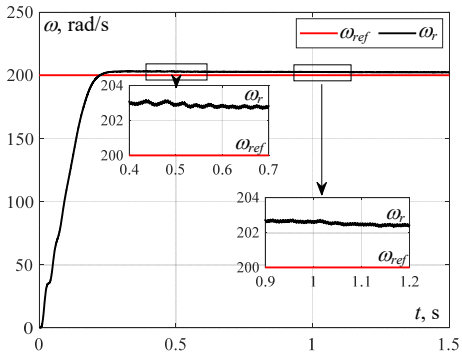

Fig. 13. Motor response under rotor resistance variations

Test 3. Phase fault evaluation. In the final test phase, the motor will start with a load torque 10 N·m, followed by the introduction of a phase fault at 1.5 s (V_a = 0), which represents challenging conditions, with a speed reference of 300 rad/s (Fig. 14). Despite the phase fault and the load torque, one can see that the DSIM continues operating with a speed value equal to 299 rad/s, ensuring service continuity. Additionally, small ripples of approximately ±1 rad/s around the reference speed are observed, highlighting the system's ability to maintain stability even under challenging and degraded conditions. The current in the faulty phase (phase A) is shown in Fig. 15. Ideally, the current in phase A should be 0, but due to interactions of magnetic fluxes, a current is induced in phase A. This phenomenon can be explained by mutual inductance, where the changing magnetic field produced by currents in other phases induces a current in the faulty phase.

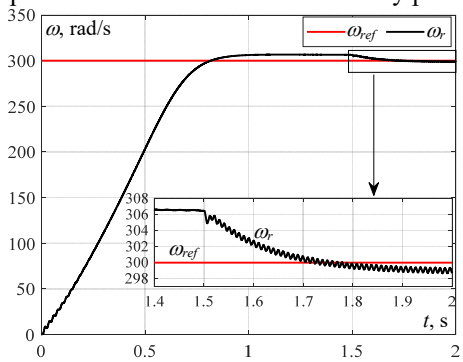

Fig. 14. Speed under load torque and phase fault

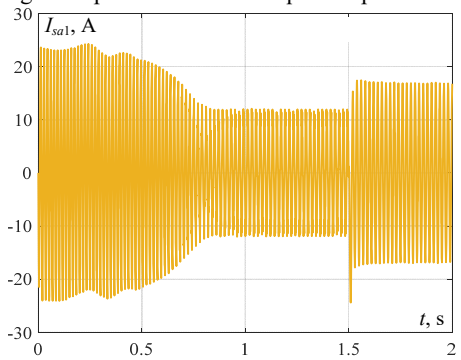

Fig. 15. Fault phase current I_{sa1}

Conclusions. The evaluation of the Linear Quadratic Regulator (LQR) applied to the dual star induction motor system (DSIM) through a series of rigorous tests has yielded promising results. In the precision test, the LQR regulator showcased high accuracy in tracking reference speed changes with zero overshoot and swift stabilization times, ensuring precise control. Furthermore, the robustness test against parameter variations demonstrated the regulator's resilience, maintaining stable motor performance even with doubled stator and rotor resistances and inertia. Additionally, the introduction of load torque displayed the system's ability to swiftly adapt while sustaining stable performance. Moreover, in the face of a phase fault and load torque at the same time, the DSIM maintained almost the same speed, with minor fluctuations around the reference speed, ensuring service continuity and stability. These results affirm the effectiveness and reliability of the LQR regulator and the DSIM in facilitating precise control and stability applications, without the need for simplifying assumptions, thereby contributing to the advancement of electric vehicle technology.

For further developments to enhance this technique, adaptive control algorithms such as fuzzy logic or neural networks can be used to improve precision and settling time by changing current classical PI regulators by one of the adaptive algorithms.

Conflict of interest. The authors declare that they have no conflicts of interest.

REFERENCES

1. Lasocki J., Krawczyk P., Kopczyński A., Roszczyk P., Hajduga A. Analysis of the strategies for managing extended-range electric vehicle powertrain in the urban driving cycle. *Electrical Engineering & Electromechanics*, 2022, no. 1, pp. 70-76. doi: https://doi.org/10.20998/2074-272X.2022.1.10.

2. Zhu X., Zhang H., Xi J., Wang J., Fang Z. Robust speed synchronization control for clutchless automated manual transmission systems in electric vehicles. *Proceedings of the Institution of Mechanical Engineers, Part D: Journal of Automobile Engineering*, 2015, vol. 229, no. 4, pp. 424-436. doi: https://doi.org/10.1177/0954407014546431.

3. Bhavik Brahmbhatt C.K.B. Indirect Field Oriented Control of Induction Motor. *Journal of Electrical Systems*, 2024, vol. 20, no. 3s, pp. 2013-2021. doi: https://doi.org/10.52783/jes.1793.

4. Kuczmann M., Horváth K. Tensor Product Alternatives for Nonlinear Field-Oriented Control of Induction Machines. *Electronics*, 2024, vol. 13, no. 7, art. no. 1405. doi: https://doi.org/10.3390/electronics13071405.

5. Phuong Duy Nguyen, An Van Vo, Thanh Lam Le, Giang Tuyet Thi Lai. Field-oriented control strategy for induction motor drives. *Proceedings of Eastern International University Scientific Conference (EIUSC 2023)*, 2023, pp. 438-445.

6. Ahmed H., Zaidi S.H., Khan F. A Comparative Study on Different Motors used in Electric Vehicles. *Journal of Independent Studies and Research Computing*, 2022, vol. 20, no. 2, pp. 32-39. doi: https://doi.org/10.31645/JISRC.22.20.2.5.

7. Ansari A.A. A Review of Different Motor Types and Selection of One Optimal Motor for Application in EV Industry. *International Journal of Electrical and Power Engineering*, 2022, vol. 16, no. 1, pp. 1-7.

8. Volkov V.A., Antonov N.L. Refined calculation of energy modes of a frequency-regulated induction motor. *Electrical Engineering & Electromechanics*, 2024, no. 5, pp. 3-13. doi: https://doi.org/10.20998/2074-272X.2024.5.01.

9. Yildirim M., Polat M., Kurum H. A survey on comparison of electric motor types and drives used for electric vehicles. *2014 16th International Power Electronics and Motion Control Conference and Exposition*, 2014, pp. 218-223. doi: https://doi.org/10.1109/EPEPEMC.2014.6980715.

10. Hashemnia N., Asaei B. Comparative study of using different electric motors in the electric vehicles. *2008 18th International Conference on Electrical Machines*, 2008, pp. 1-5. doi: https://doi.org/10.1109/ICELMACH.2008.4800157.

11. Zeraoulia M., Benbouzid M.E.H., Diallo D. Electric Motor Drive Selection Issues for HEV Propulsion Systems: A Comparative Study. *IEEE Transactions on Vehicular Technology*, 2006, vol. 55, no. 6, pp. 1756-1764. doi: https://doi.org/10.1109/TVT.2006.878719.

12. Madichetty S., Mishra S., Basu M. New trends in electric motors and selection for electric vehicle propulsion systems. *IET Electrical Systems in Transportation*, 2021, vol. 11, no. 3, pp. 186-199. doi: https://doi.org/10.1049/els2.12018.

13. Khadar S., Kouzou A., Rezzaoui M.M., Hafaifa A. Sensorless Control Technique of Open-End Winding Five Phase Induction Motor under Partial Stator Winding Short-Circuit. *Periodica Polytechnica Electrical Engineering and Computer Science*, 2019, vol. 64, no. 1, pp. 2-19. doi: https://doi.org/10.3311/PPee.14306.

14. Marouani K., Baghli L., Hadiouche D., Kheloui A., Rezzoug A. A New PWM Strategy Based on a 24-Sector Vector Space Decomposition for a Six-Phase VSI-Fed Dual Stator Induction Motor. *IEEE Transactions on Industrial Electronics*, 2008, vol. 55, no. 5, pp. 1910-1920. doi: https://doi.org/10.1109/TIE.2008.918486.
15. Sellah M., Abdellah K., Rezaoui M.M. Investigation of SVPWM Based Sliding Mode Control Application on Dual-Star Induction Motor and Dual Open-End Winding Induction Motor. *Periodica Polytechnica Electrical Engineering and Computer Science*, 2022, vol. 66, no. 1, pp. 80-98. doi: https://doi.org/10.3311/PPee.17910.
16. Boukhalfa G., Belkacem S., Chikhi A., Benaggoune S. Direct torque control of dual star induction motor using a fuzzy-PSO hybrid approach. *Applied Computing and Informatics*, 2022, vol. 18, no. 1/2, pp. 74-89. doi: https://doi.org/10.1016/j.aci.2018.09.001.
17. Pieńkowski K. Analysis and control of dual stator winding induction motor. *Archives of Electrical Engineering*, 2012, vol. 61, no. 3, pp. 421-438. doi: https://doi.org/10.2478/v10171-012-0033-z.
18. Bouziane M., Abdelkader M. A Neural Network Based Speed Control of a Dual Star Induction Motor. *International Journal of Electrical and Computer Engineering (IJECE)*, 2014, vol. 4, no. 6. pp. 952-961. doi: https://doi.org/10.11591/ijece.v4i6.6343.
19. Layadi N., Djerioui A., Zeghlache S., Houari A., Benkhoris M.-F., Berrabah F. A Hybrid Fuzzy Sliding Mode Controller for a Double Star Induction Machine. *2018 International Conference on Communications and Electrical Engineering (ICCEE)*, 2018, pp. 1-6. doi: https://doi.org/10.1109/CCEE.2018.8634439.
20. Hadiouche D., Baghli L., Rezzoug A. Space-vector PWM techniques for dual three-phase AC machine: analysis, performance evaluation, and DSP implementation. *IEEE Transactions on Industry Applications*, 2006, vol. 42, no. 4, pp. 1112-1122. doi: https://doi.org/10.1109/TIA.2006.877737.
21. Boukhalfa G., Belkacem S., Chikhi A., Bouhentala M. Fuzzy-second order sliding mode control optimized by genetic algorithm applied in direct torque control of dual star induction motor. *Journal of Central South University*, 2022, vol. 29, no. 12, pp. 3974-3985. doi: https://doi.org/10.1007/s11771-022-5028-3.
22. Benayache R. *Contribution à la commande robuste des systèmes non linéaires incertains application à un système hydraulique*. Thèse de doctorat, Université de Valenciennes et du Hainaut Cambrésis, France, 2007. 200 p. (Fra).
23. Yunfei L., Chengning Z. A Comparative Experimental Analysis of PMSM between Deadbeat Prediction Current Control and Field-oriented Control. *Energy Procedia*, 2019, vol. 158, pp. 2488-2493. doi: https://doi.org/10.1016/j.egypro.2019.01.382.
24. Guo Z., Zhang J., Sun Z., Zheng C. Indirect Field Oriented Control of Three-phase Induction Motor Based on Current-source Inverter. *Procedia Engineering*, 2017, vol. 174, pp. 588-594. doi: https://doi.org/10.1016/j.proeng.2017.01.192.
25. Akyol I.E., Soylemez M.T. Position Sensorless Field Oriented Control of IPMSM Under Parameter Uncertainties. *IFAC-PapersOnLine*, 2017, vol. 50, no. 1, pp. 14501-14506. doi: https://doi.org/10.1016/j.ifacol.2017.08.2301.
26. Bohari A.A., Utomo W.M., Haron Z.A., Zin N.M., Sim S.Y., Ariff R.M. Speed Tracking of Indirect Field Oriented Control Induction Motor Using Neural Network. *Procedia Technology*, 2013, vol. 11, pp. 141-146. doi: https://doi.org/10.1016/j.protcy.2013.12.173.
27. Chang G.W., Hespanha J.P., Morse A.S., Netto M.S., Ortega R. Supervisory field-oriented control of induction motors with uncertain rotor resistance. *International Journal of Adaptive Control and Signal Processing*, 2001, vol. 15, no. 3, pp. 353-375. doi: https://doi.org/10.1002/acs.671.
28. Pradeep Kumar M., Sirisha S., Chandramouly M. Design of PMSM base on DTC method with MRAS. *International Journal of Engineering Research and Applications*, 2013, vol. 3, no. 5, pp. 282-287.
29. Alwi H., Edwards C., Pin Tan C. *Fault Detection and Fault-Tolerant Control Using Sliding Modes*. Springer London, 2011. 340 p. doi: https://doi.org/10.1007/978-0-85729-650-4.
30. Li X., Zhang Z., An J., Zhou X., Hu G., Zhang G., Man W. Adaptive sliding mode control of modular self-reconfigurable spacecraft with time-delay estimation. *Defence Technology*, 2022, vol. 18, no. 12, pp. 2170-2180. doi: https://doi.org/10.1016/j.dt.2021.12.005.
31. Pal P., Jin G.G., Bhakta S., Mukherjee V. Adaptive chaos synchronization of an attitude control of satellite: A backstepping based sliding mode approach. *Heliyon*, 2022, vol. 8, no. 11, art. no. e11730. doi: https://doi.org/10.1016/j.heliyon.2022.e11730.
32. Ibrar A., Ahmad S., Safdar A., Haroon N. Efficiency enhancement strategy implementation in hybrid electric vehicles using sliding mode control. *Electrical Engineering & Electromechanics*, 2023, no. 1, pp. 10-19. doi: https://doi.org/10.20998/2074-272X.2023.1.02.
33. Li H.Y., Hu Y.A. Robust sliding-mode backstepping design for synchronization control of cross-strict feedback hyperchaotic systems with unmatched uncertainties. *Communications in Nonlinear Science and Numerical Simulation*, 2011, vol. 16, no. 10, pp. 3904-3913. doi: https://doi.org/10.1016/j.cnsns.2011.02.031.
34. Prasad K.M.A., Unnikrishnan A., Nair U. Fuzzy Sliding Mode Control of a Switched Reluctance Motor. *Procedia Technology*, 2016, vol. 25, pp. 735-742. doi: https://doi.org/10.1016/j.protcy.2016.08.167.
35. Najim K. *Commande adaptative des processus industriels*. Masson, Paris, 1997. 120 p. (Fra).
36. Nguyen N.T. *Model-Reference Adaptive Control*. Springer International Publishing, 2018. 444 p. doi: https://doi.org/10.1007/978-3-319-56393-0.
37. Alekseev V., Tikhomirov V., Fomin S. *Optimal control*. Moscow, Mir Publ., 1982. 447 p. (Rus).
38. Wu S., Zhang R. Improved LQ Tracking Control Design for Industrial Processes Under Uncertainty: The Extended Nonminimal State Space Approach. *IEEE Transactions on Systems, Man, and Cybernetics: Systems*, 2022, vol. 52, no. 2, pp. 1356-1360. doi: https://doi.org/10.1109/TSMC.2020.3014839.
39. Elkhatem A.S., Engin S.N. Robust LQR and LQR-PI control strategies based on adaptive weighting matrix selection for a UAV position and attitude tracking control. *Alexandria Engineering Journal*, 2022, vol. 61, no. 8, pp. 6275-6292. doi: https://doi.org/10.1016/j.aej.2021.11.057.
40. Khemis A., Boutabba T., Drid S. Model reference adaptive system speed estimator based on type-1 and type-2 fuzzy logic sensorless control of electrical vehicle with electrical differential. *Electrical Engineering & Electromechanics*, 2023, no. 4, pp. 19-25. doi: https://doi.org/10.20998/2074-272X.2023.4.03.
41. Yin Y., Liu L., Hu Z., Lin H., Wu L. Adaptive Optimal Control for PMSM Servo System. *Lecture Notes in Electrical Engineering*, 2024, vol. 1034, pp. 131-151. doi: https://doi.org/10.1007/978-3-031-53188-0_7.
42. El-samahy A.A., Shamseldin M.A. Brushless DC motor tracking control using self-tuning fuzzy PID control and model reference adaptive control. *Ain Shams Engineering Journal*, 2018, vol. 9, no. 3, pp. 341-352. doi: https://doi.org/10.1016/j.asej.2016.02.004.
43. Rajesh R., Deepa S.N. Design of direct MRAC augmented with 2 DoF PIDD controller: An application to speed control of a servo plant. *Journal of King Saud University - Engineering Sciences*, 2020, vol. 32, no. 5, pp. 310-320. doi: https://doi.org/10.1016/j.jksues.2019.02.005.
44. Ganesh V., Vasu K., Bhavana P. LQR based load frequency controller for two area power system. *International Journal of Advanced Research in Electrical, Electronics and Instrumentation Engineering*, 2012, vol. 1, no. 4, pp. 262-269.

Received 06.07.2024
Accepted 13.09.2024
Published 02.03.2025

Z. Darsouni [1], *PhD Student,*
S.E. Rezgui [1], *Doctor of Technical Science,*
H. Benalla [1], *Professor,*
F. Rebahi [2], *Doctor of Technical Science,*
M.A.M. Boumendjel [1], *PhD Student,*
[1] Laboratory of Electrical Engineering of Constantine (LEC), Technology Sciences Faculty,
University Freres Mentouri Constantine 1, Algeria,
e-mail: darsounizakaria@gmail.com (Corresponding Author).
[2] Department of Electronic, Electrical Engineering and Automatic, National Polytechnic School of Constantine, Algeria.

How to cite this article:
Darsouni Z., Rezgui S.E., Benalla H., Rebahi F., Boumandjel M.A.M. Ensuring service continuity in electric vehicles with vector control and linear quadratic regulator for dual star induction motors. *Electrical Engineering & Electromechanics*, 2025, no. 2, pp. 24-30. doi: https://doi.org/10.20998/2074-272X.2025.2.04